Mon. Not. R. Astron. Soc. **000**, 000–000 (0000) Printed 2 September 2014 (MN LATEX style file v2.2)

ISIMA report on: Torque on an exoplanet from an anisotropic evaporative wind

Jean Teyssandier[1,2], James E. Owen[3], Fred C. Adams[4,5], & Alice C. Quillen[6]

[1] *Institut d'Astrophysique de Paris, UPMC Univ Paris 06, CNRS, UMR7095, 98 bis bd Arago, F-75014, Paris, France*

[2] *Department of Astrophysics, University of Oxford, Keble Road, Oxford OX1 3RH, England*

[3] *Canadian Institute for Theoretical Astrophysics, University of Toronto, 60 St. George Street, Toronto, Ontario, Canada*

[4] *Michigan Center for Theoretical Physics Physics Department, University of Michigan, Ann Arbor, MI 48109, USA*

[5] *Astronomy Department, University of Michigan, Ann Arbor, MI 48109, USA*

[6] *Department of Physics and Astronomy, University of Rochester, Rochester, NY 14627, USA*

2 September 2014

ABSTRACT

Winds from short-period Earth and Neptune mass exoplanets, driven by X-ray and EUV radiation from a young star, may evaporate a significant fraction of a planet's mass. If the momentum flux from the evaporative wind is not aligned with the planet/star axis, then it can exert a torque on the planet's orbit. Using steady-state one-dimensional evaporative wind models by Owen & Jackson (2012), we estimate this torque using a lag angle that depends on the product of the speed of the planet's upper atmosphere and a flow timescale for the wind to reach its sonic radius. We also estimate the momentum flux from time-dependent one-dimensional hydrodynamical simulations. We find that only in a very narrow regime in planet radius, mass and stellar radiation flux is a wind capable of exerting a significant torque on the planet's orbit. A close-in super Earth mass planet that loses a large fraction of its mass in a wind could drift a few percent of its semi-major axis. While this is small, it can places constraint on the evolution of resonant pairs such as Kepler 36 b and c. Similar to the Yarkovsky effect, a wind causes the planet to drift outward if atmospheric circulation is prograde (super-rotating) and vice versa if the circulation is retrograde.

1 INTRODUCTION

Planets discovered by the Kepler Observatory (Batalha et al. 2013) exhibit a large range of densities ranging from less than 1 g cm^{-3} (Kepler 36c; Carter et al. 2012 and Kepler 79d, Jontof-Hutter et al. 2014) to greater than 8 g cm^{-3} (Kepler 10b, Batalha et al. 2011). For Neptune and Earth mass planets, inferred gaseous envelope masses range from zeros to tens of percent of the total planetary mass, with this fraction being dependent on whether a rock/iron or ice core is adopted (Howe et al. 2014). Either close-in planets are formed with a wide range of core to envelope mass ratios, or their compositions evolve after they have accreted gas (and after evaporation of the circumstellar disk). Evaporative winds driven by stellar UV and X-ray radiation could account for the loss of a significant fraction of a Neptune-sized planet's gaseous envelope mass (Lopez & Fortney 2013; Owen & Wu 2013). Impacts or collisions between bodies that are more frequent at small semi-major axis can also affect the planetary composition (e.g., Quillen et al. 2013). Among planet pairs in multiple-planet systems, a larger fraction ($\sim 60\%$) of systems have the smaller radius planet residing closer to the star (Ciardi et al. 2013). As more mass can be evaporated closer to a star, evaporative winds could account for this trend (Owen & Wu 2013).

In addition, evidence for mass loss through atmospheric evaporation have been observed for the hot Jupiters around HD 209458 (Vidal-Madjar et al. 2003) and HD 189733 (Lecavelier des Etangs et al. 2010), with loss rates estimated to be of the order of 10^{10} g s^{-1}.

An evaporative wind from an exoplanet is often assumed to be isotropic. However, an evaporative wind carries momentum and could exert a torque on the planet affecting both its orbit and spin. Here we first summarize related physical phenomena. Veras et al. (2013) showed that an anisotropic stellar wind can cause orbital inclination changes. Also of interest, the Yarkovsky effect is where uneven re-emission of absorbed stellar radiation causes drifts in asteroid semi-major axes (see Bottke et al. 2006). It has also been shown that sublimation from a comet can exert a reactive torque on the cometary nucleus (Gutiérrez et al. 2002; Neishtadt et al. 2003). Boué et al. (2012) proposed that an anisotropy in an evaporative wind from a close-in Jupiter- or Neptune-mass planet can cause the planet's orbit to migrate (see also Iorio 2012). Boué et al. (2012) suggested that migration distances inferred from distributions of planetary mass and orbits could be used to constrain the launch angle of the evaporative wind. Here we attempt to estimate the launch angle of the wind and magnitude of the resulting reactive torque on the planet based on hydrodynamical models.

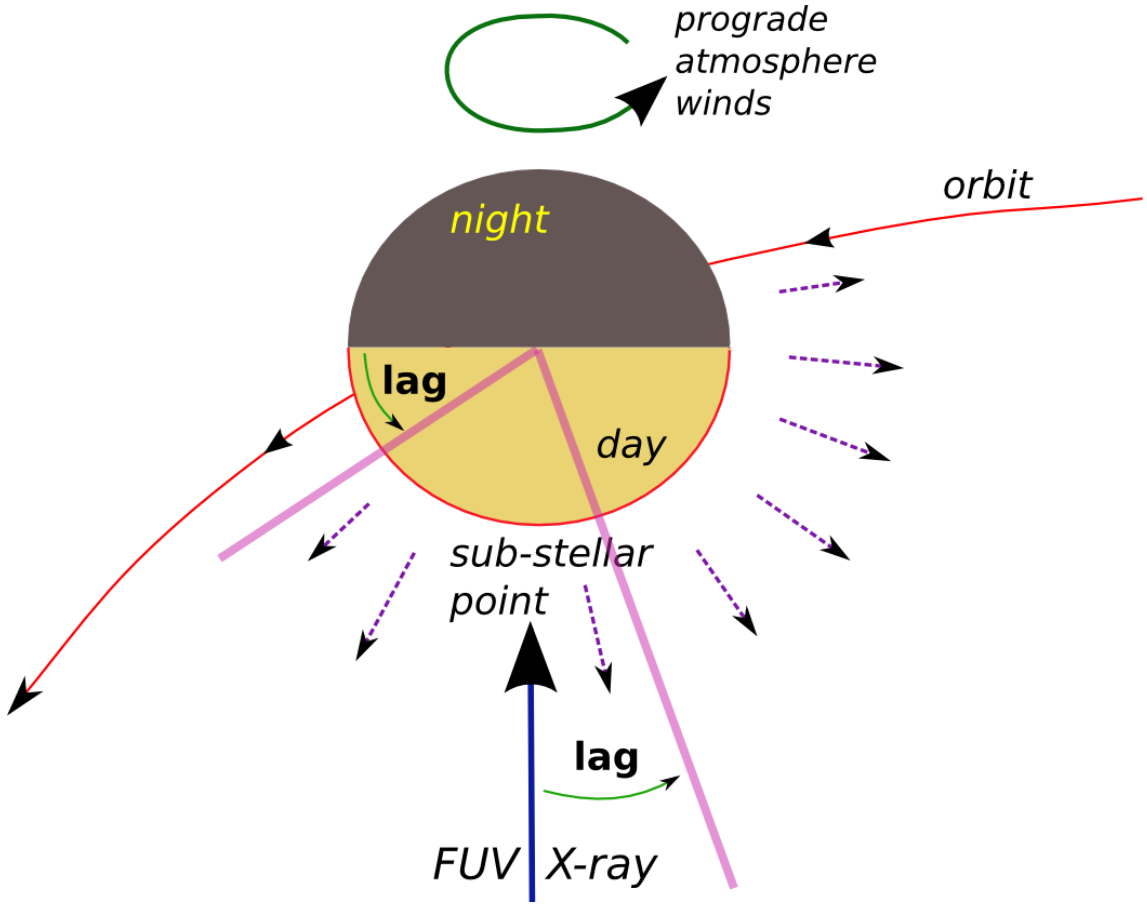

Figure 1. If the wind launch region is super-rotating with respect to a tidally locked planet, then the wind is launched after the upper atmosphere sees dawn. A comparison between a timescale to launch the wind and the rotation rate of the upper atmosphere gives an angular lag in the peak of the day-driven wind. Because of the lag, the momentum flux of the wind is offset compared to the star/planet axis and this gives a torque on the planet. If the upper atmosphere is super-rotating with respect to the planet, the torque increases the angular momentum of the planet and the planet's orbit moves outward.

As evaporation is primarily significant for low core mass planets experiencing high UV and X-ray fluxes (Lopez & Fortney 2013; Owen & Wu 2013) from the star, we focus here on winds driven from Neptune and Earth-mass planets within 0.2 AU of a star.

As the cooling timescale in an ionosphere is expected to be shorter than a day, an evaporative wind is mainly expected to be driven from the day side of a planet. If the planet is not tidally locked or if the atmosphere is circulating then the upper atmosphere would experience day/night variations in stellar illumination. A delay between dawn and the time it takes for the wind to develop could cause an asymmetry in the wind (see Figure 1). Here we estimate the torque on a planet due to this possible asymmetry.

Planets within 0.2 AU are expected to be tidally locked and at low obliquity (e.g., Lubow et al. 1997; Cunha et al. 2014). Spin-down should have taken place in less than $\sim 10^4$ years (see Table 1 by Cunha et al. 2014), and well before the time when most of the evaporation takes place, at an age $\sim 10^7 - 10^8$ years (Owen & Jackson 2012). However,

some planets could now be in a spin synchronous state (with rotation rate related to the angular rotation rate at pericenter, Hut 1981) or spin-orbit resonance (Rodriguez et al. 2012) like Mercury. Even though the tidal spin-down timescale is short, the timescale for tidal circularization of the orbit is relatively long (e.g., Ford & Rasio 2008; Lee et al. 2013) and planets could have been at moderate (or their current) eccentricities when atmospheric evaporation took place. About a quarter of the planets in multiple-planet Kepler systems with transit-timing variations have high eccentricities, in the range 0.1-0.4 (Wu & Lithwick 2013). In exoplanetary systems containing at least two planets, transit timing variations are consistent with an eccentricity dispersion of $0.018^{+0.005}_{-0.004}$ when fit with a Rayleigh distribution (Hadden & Lithwick 2014).

Even if a planet is tidally locked, the upper atmosphere can be super-rotating with advective or zonal flow speeds of order $v_{zonal} \sim 1$ km/s (Showman & Polvani 2011; Menou 2012; Rauscher & Kempton 2014). If the advective flow speed scales with the sound speed (e.g., Cowan & Agol 2011b) then we expect a wind speed $\propto T_{eq}^{1/2}$, where T_{eq} is the equilibrium temperature set by radiation balance from the stellar light. As this is weakly dependent on the planet's semi-major axis ($T_{eq} \propto a_p^{-1/2}$ with a_p the semi-major axis of the planet) we can neglect the possible dependence of advective flow speed on stellar flux and planet properties such as atmospheric opacity and surface gravity. Evaporative winds are driven from a tenuous region of a planetary atmosphere where ionization occurs, and this is higher than typically modeled to predict atmospheric circulation. Nevertheless 1 km/s size-scale zonal flows are predicted in exoplanet ionospheres (see Figure 3 by Koskinen et al. 2010).

Both zonal circulation or a spin-orbit resonance would cause a planetary ionosphere to experience day/night variations. In section 2 we estimate a torque due to an evaporative wind by considering the relationship between atmospheric motion and the timescale to launch a wind at dawn. In section 3 we compute a lag angle for the wind momentum loss rate using one-dimensional hydrodynamical steady-state evaporative wind models (Owen & Jackson 2012). In section 4 we compute this angle by integrating one dimensional but time-dependent hydrodynamic models. Lastly in 5 we investigate scenarios for the Kepler 36 planetary system taking into account an evaporative wind induced torque. Variations in the planet's orbital elements, integrated over the orbit, are computed in the appendix.

For completeness, we note that, in addition to the effects outlined above, magnetic fields on the planetary surface will lead to anisotropy. More specifically, with the expected mass loss

rates from planets and surface field strengths of ~ 1 gauss, the outflows will be magnetically controlled (Owen & Adams 2014). This issue must be addressed in future work.

2 TORQUE ESTIMATE AND LAG ANGLE

Stellar X-ray and EUV radiation heats gas up to temperatures $T \sim 10^4$ K (Spitzer 1978; Shu 1992) corresponding to a sound speed of $c_{EUV} \sim 10$ km/s. Above this temperature radiative cooling is so efficient that higher temperatures are rarely reached. As c_{EUV} is similar to a planet's escape velocity, a wind can be launched from the heated gas. An isothermal or Parker-type wind model (Parker 1958, 1965) gives an approximate hydrodynamical description for evaporative winds from close-in planets (Owen & Jackson 2012). Such a wind cannot be instantaneously launched at dawn. We can estimate a launch timescale for the wind from the time it takes for a particle in the wind to travel from the planet's surface, at a planetary radius R_p, to the transonic radius, R_s,

$$t_{flow} \sim \int_{R_p}^{R_s} \frac{dr}{u} \sim \frac{R_s}{c_{EUV}} \tag{1}$$

where u is the wind velocity as a function of radius. An isothermal spherically symmetric steady-state wind model (e.g., Cranmer 2004) gives

$$R_s \sim \frac{GM_p}{2c_{EUV}^2} \tag{2}$$

and

$$t_{flow} \sim \frac{GM_p}{2c_{EUV}^3} \sim 200 \text{ s} \left(\frac{M_p}{M_\oplus}\right) \left(\frac{c_{EUV}}{10 \text{ km s}^{-1}}\right)^{-3}. \tag{3}$$

The one-dimensional hydrodynamic models that include ionization by Owen & Jackson (2012) have $R_s \sim 2 - 3R_p$ (see their Figure 4) where R_p is the planet's radius. Using these larger transonic radii we find:

$$t_{flow} \sim \frac{R_s}{c_{EUV}} \sim 640 \ s \left(\frac{R_p}{R_\oplus}\right) \left(\frac{R_s/R_p}{2}\right) \left(\frac{c_{EUV}}{10 \text{ km s}^{-1}}\right)^{-1}. \tag{4}$$

The motion of the upper atmosphere wind, described by a zonal wind speed z_{zonal}, and the timescale to launch the wind together imply that the wind is not launched at dawn but slightly afterwards. It would take a similar time for the evaporative wind to die down after dusk. The delay implies that the average wind momentum is not pointing exactly toward the star along the sub-stellar point but is shifted by an angle θ_{lag} from this direction (see Figure 1). We estimate this angle

$$\theta_{lag} \sim \frac{t_{flow}}{t_{zonal}}, \tag{5}$$

where

$$t_{zonal} = \frac{R_p}{v_{zonal}} = 637\text{s} \left(\frac{v_{zonal}}{1\text{km s}^{-1}} \right)^{-1} \left(\frac{R_p}{R_\oplus} \right) \quad (6)$$

is the inverse of the atmosphere's angular rotation rate. A comparison between equation (6) and equation (4) suggests that the angle θ_{lag} could be of order 1 and the wind could exert a significant torque on the planet. If $t_{flow} \gg R_p/v_{zonal}$ then we could consider the wind launched evenly from both day and night sides. If $t_{flow} \ll R_p/v_{zonal}$ then the momentum flux from the wind is in the radial direction and there is no torque. We have used a flow timescale to estimate the time it takes to launch the wind that is based on a steady state flow model. An alternative thermal timescale, t_{tk}, that can be used to estimate a wind launch timescale is the time it takes to replenish the kinetic energy in the flow within the sonic radius from the absorbed EUV and X-ray energy flux. Depending upon the ratio of the transonic to planet radius, and as we discuss below, a thermal timescale may more accurately describe the time it takes to launch the wind. We have neglected the wind speed's tangential velocity component in our estimate for θ_{lag} as v_{zonal} is significantly smaller than the escape velocity from the planet surface.

The orbital torque (from the wind) can be roughly estimated from the lag angle θ_{lag} as

$$\tau_w \sim \dot{M} \theta_{lag} v_w a_p / 2 \quad (7)$$

where $\dot{M}$ is the wind mass outflow rate and $v_w \sim c_{EUV}$ is a mean wind velocity near the transonic region. The rough factor of 2 comes from integrating a radial wind over a hemisphere with an angular offset.

The sign of the lag is set by the direction of planet spin or atmospheric flow. If the planet's spin or the atmospheric circulation are prograde (super-rotating or eastward) then the torque is positive and we expect the planet to move outwards. The sign is in direct analogy to the Yarkovsky effect (see Bottke et al. 2006), with outward migration in semi-major axis for prograde asteroid body rotation and vice versa for retrograde body rotation. Close-in exoplanet atmospheric circulation models usually predict prograde (super-rotating or eastward) equatorial upper atmospheric circulation (Showman & Polvani 2011; Menou 2012; Rauscher & Kempton 2014), with the exception of the retrograde (westward) slowly rotating model for HD 209458b by Rauscher & Kempton (2014).

A strong evaporative winds is driven when the host star has a strong EUV and X-ray flux or during an age less than $\Delta t \sim 10^8$ years (Owen & Jackson 2012). During this time, a planet of mass M_p can experience a loss of mass $\Delta M_p = \dot{M} \Delta t$ and a change in semi-major

axis Δa_p. The change in the planet's orbital angular momentum is

$$\Delta L \approx \tau_w \Delta t \sim M_p v_c \Delta a_p / 2, \tag{8}$$

where M_p is the planet mass and v_c the planet's orbital velocity (for assuming a nearly circular orbit), which scales as

$$v_c = 94\text{km s}^{-1} \left(\frac{M_*}{M_\odot}\right)^{\frac{1}{2}} \left(\frac{a_p}{0.1\text{ AU}}\right)^{-\frac{1}{2}}. \tag{9}$$

Using equation (7) for the torque, we estimate

$$\frac{\Delta a_p}{a_p} \sim \frac{\dot{M}\Delta t}{M_p}\frac{v_w}{v_c}\theta_{lag} \sim \frac{\Delta M_p}{M_p}\frac{v_w}{v_c}\theta_{lag} \tag{10}$$

The factor v_w/v_c limits the size-scale of the possible migration distance in semi-major axis.

Many of the Kepler planet host stars have masses lower than $1M_\odot$ (Batalha et al. 2013) and for these lower mass stars the ratio v_w/v_c would be higher. Previous studies (Owen & Wu 2013; Lopez & Fortney 2013) have found that close-in low core mass planets can loose a significant fraction of their mass. Taking $\Delta M_p/M_p \sim 1$ and $\theta_{lag} \sim 1$, Equation (10) gives

$$\frac{\Delta a_p}{a_p} \sim 0.1\frac{\Delta M_p}{M_p}\theta_{lag}\left(\frac{v_w}{10\text{ km s}^{-1}}\right)\left(\frac{M_*}{M_\odot}\right)^{\frac{1}{2}}\left(\frac{a_p}{0.1\text{ AU}}\right)^{-\frac{1}{2}}. \tag{11}$$

A planet that loses a significant fraction of its mass could move a significant fraction (say 10%) of its semi-major axis. 10% exceeds the distance to resonance exhibited by resonant pairs Fabrycky et al. (2014) and is dynamically significant, particularly for close resonant pairs such as Kepler 36b,c (Carter et al. 2012).

3 LAG ANGLE ESTIMATED FROM STEADY-STATE MODELS

In the previous section we estimated the torque on a planet due to evaporative wind loss using a crudely estimated launch timescale for the wind. In this section we use the steady-state hydrodynamic models, including radiative cooling and ionization, by Owen & Jackson (2012) to better estimate the lag angle θ_{lag} that sets the torque from the wind.

Assuming an isothermal gas

$$P = c_{EUV}^2 \rho \tag{12}$$

and spherically symmetric mass loss:

$$\dot{M} = 4\pi r^2 \rho u, \tag{13}$$

the steady-state Euler equation is

$$u\frac{\partial u}{\partial r} = -\frac{1}{\rho}\frac{\partial P}{\partial r} - \frac{GM_p}{r^2} = -\frac{c_{EUV}^2}{\rho}\frac{\partial \rho}{\partial r} - \frac{GM_p}{r^2} \tag{14}$$

Following Cranmer (2004) one can solve this set of equations for the Mach number $\mathcal{M} = u/c_s$ as a function of radius. The transonic radius is $R_s = GM_p/(2c_{EUV}^2)$, and for $r < R_s$

$$\mathcal{M}(r) = \sqrt{-W_0(-y)}, \tag{15}$$

where W_0 is the Lambert-W function and

$$y = \left(\frac{r}{R_s}\right)^{-4} \exp\left(3 - 4\frac{R_s}{r}\right). \tag{16}$$

The time for the wind to travel from the planetary surface R_p to the transonic radius R_s is

$$t_{flow} \equiv \frac{R_p}{c_{EUV}} \int_1^{R_s/R_p} \frac{1}{\mathcal{M}} \mathrm{d}\xi \tag{17}$$

with $\xi = r/R_p$.

The sonic radius as a function of the planetary radius and planetary mass is tabulated by Owen & Jackson (2012). For each pair of planetary radius and mass, we can integrate eq. (17). We compare it to t_{zonal} (equation [6]) using a zonal flow velocity of $v_{zonal} = 1$ km/s on figure 2.

An isothermal wind has a transonic radius at

$$R_s = \frac{GM_p}{2c_{EUV}^2} = 0.3R_\oplus \left(\frac{M_p}{M_\oplus}\right) \tag{18}$$

and this can be smaller than the transonic radius predicted by Owen & Jackson (2012). Even though the transonic wind radius predicted from a steady-state isothermal model does not agree with those calculated by Owen & Jackson (2012), we use equation (17) to predict the flow timescale to the transonic radius and we use the transonic radii calculated by Owen & Jackson (2012), assuming that the isothermal wind flow model has approximately the correct form.

We can also estimate the time it takes to heat the wind from a ratio of kinetic energy (integrated out to the sonic radius, $\sim \rho_s c_{EUV}^2 4\pi R_s^3/3$) and the energy absorbed per unit time in UV and X-ray photons, $\sim \pi R_p^2 F_{UV}$ where ρ_s is the density in the wind at R_s and F_{UV} is the flux in X-ray and EUV photons from the star. In analogy to the Kelvin-Helmholtz timescale we write

$$t_{kh} = \frac{\int 4\pi r^2 dr \rho u^2}{\pi R_p^2 F_{UV}}, \tag{19}$$

where the numerator represents represents the integral of the energy density in the flow over the volume within the sonic radius. Using the continuity equation $\dot{M} = 4\pi r^2 \rho u = constant$ and noting that the conservation of energy implies $\dot{M} = \eta\pi R_p^3 F_{UV}/GM_p$ (with $\eta < 1$ the

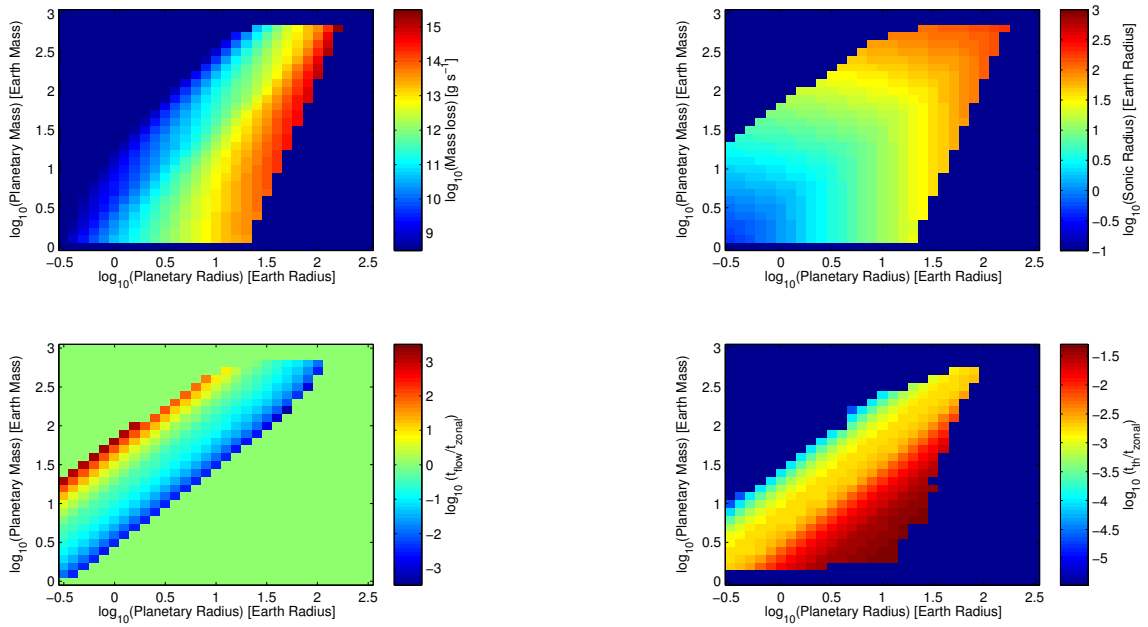

Figure 2. top left: mass loss from Owen & Jackson 2012. Top right: Sonic radius from Owen & Jackson 2012. Bottom left: t_{flow}/t_{zonal} as given by eq. (17). Bottom right: t_{KH}/t_{zonal} as given by eq. (20). All for an X-ray + EUV stellar luminosity of 10^{30} erg/s and a semi-major axis of 0.1 AU.

efficiency factor), we write the Kelvin-Helmholtz timescale as

$$t_{kh} = \frac{\eta}{b}\frac{R_p}{c_{EUV}}\int_1^{R_s/R_p} u d\xi, \tag{20}$$

with $b = GM_p/R_p c_{EUV}^2$. On figure 2 we also give the Kelvin-Helmoltz timescale (bottom right panel), where we have arbitrarily taken $\eta = 0.25$.

The tow top panels of Figure 2 show the mass loss and sonic radius as computed by Owen & Jackson (2012). There is no solution in the left part because of Roche lob overflow. In addition there is no solution in the right corner because in this region, there is no solution possible for hydrodynamical escape. Figure 2 shows that the flow timescale is long at low surface gravities (top left) and short at high surface gravity (bottom right). On the bottom right the transonic radius is very close to the planet radius and our flow timescale gives an unrealistic estimate of the time it takes to launch the wind.

Looking at Figure 2 we confirm that there is a region where both mass loss is important and where the lag angle is of order 1. This implies that strong evaporative winds from low mass close-in exoplanets could exert a significant torque on the planet. Probably this only occurs in a narrow region of M_p and R_p space at a given F_{UV}.

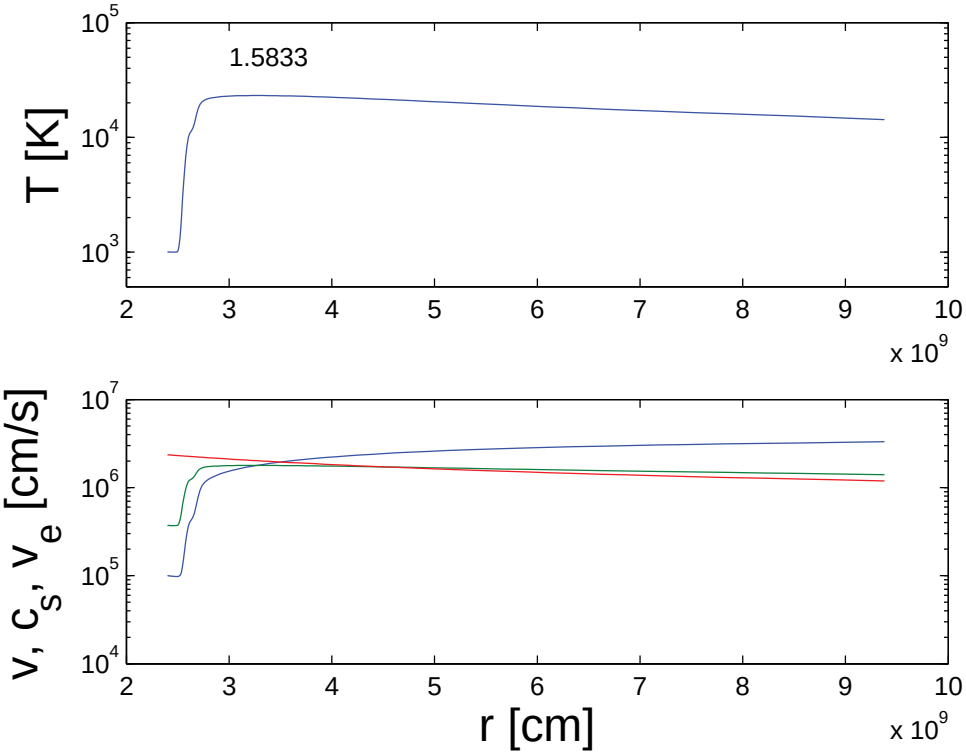

Figure 3. Flow solution at a longitude of 1.5833 rad (near the substellar point). Top panel: Temperature profile. Bottom panel: total speed (blue curve), sound speed (green curve) and escape velocity (red curve). For all four plots, the x axis is the radial distance. The planetary radius is that of Neptune, i.e. 2.4 10^9 cm.

4 MOMENTUM LOSS RATE ESTIMATED FROM ONE-DIMENSIONAL TIME DEPENDENT HYDRODYNAMICAL MODELS

To improve on the estimates that are based on the steady-state models in section 3 we carry out some one dimensional but time-dependent hydrodynamic models. From these we directly estimate the lag angle and the vector direction of the momentum carried by the evaporative wind.

We conduct a set of 1+1D simulations using ZEUS (Stone & Norman 1992), where we irradiate a small patch at the surface of the planet with a UV flux. We add a longitudinal dependence for the UV flux. First, we study a Neptune-like planet, with a radius of 2.4×10^9 cm and a mass of 1.03×10^{29} g. It is irradiated with a flux of 2×10^6 erg s^{-1} cm^{-2}. This corresponds to a planet at 0.013 AU from a star with a X-Ray and UV luminosity of 10^{30} erg s^{-1}.

From the temperature profile we derive the local sound speed. We identify the sonic point from the location where the flow speed becomes supersonic. In figure 3 we give a snapshot of the flow solution near the stellar point (given by a longitude $\phi = \pi/2$).

In figure 4 we show the sonic surface as a function of the longitude, taken at the equator, on the day-side only. As expected, the sonic point is close to the planetary surface around the substellar point. However, the minimum of the curve appears to be offset from the substellar point by a few degrees. In figure 5 we show the sonic point for different lattitudes and longitudes, for the same configuration as figure 4. We estimate that, at the equator, the minimum sonic radius is offset from the sub-stellar point by 16° westward.

From this set of simulation, we can also extract the total mass loss, integrated over the longitudes ϕ and latitudes θ, at an altitude r (e.g., the sonic radius). It reads:

$$\dot{M} = \int_{\theta=-\pi/2}^{\pi/2} \int_{\phi=0}^{2\pi} \sin\theta \mathrm{d}\theta \mathrm{d}\phi \rho(r,\theta,\phi) v(r,\theta,\phi) r^2. \quad (21)$$

In this case we find it to be 2.4 10^{12} g s^{-1}.

Another relevant quantity is the the momentum loss rate of the wind, $\dot{\mathbf{P}}$, which we explicitly give in appendix B. It is a vector, which we give in the following reference frame: the origin is at the substellar point, the x direction lies along the line that goes from the substellar point the the star, the y axis is perpendicular to the x axis along the equator in the east direction, and the z is perpendicular to the equator in the north direction. The problem is symmetric with regard to the planet's equator, so that the z contribution cancels out once integrated over the whole planetary surface. We estimate the lag angle of the wind θ_{lag} through the relation $\tan\theta_{lag} = \dot{P}_y/\dot{P}_x$. In this case we find $\theta_{lag} = +12°$.

Our one dimensional time-dependent model has therefore allowed us to show that a short-period, strongly irradiated, Neptune-like planet, looses mass at rate similar to other studies. In addition the momentum flux indicates that mass loss is anisotropic, and occurs at an angle that is offset from the substellar point by a few tenths of radians. According to our estimate in equation (10), this would shift the semi-major axis of the planet by less than 0.1%.

5 APPLICATION TO KEPLER 36

5.1 Hydrodynamical escape

Lopez & Fortney (2013) have found that the peculiar architecture of the Kepler 36 system can be reproduced by evaporation of a pair of planets with cores of 4.45 $M_\oplus$ (inner planet) 7.34 $M_\oplus$ and (outer planet). Both cores are surrounded by a gaseous atmosphere, which initially contains about 23% of the total mass of the planet in the form of hydrogen and

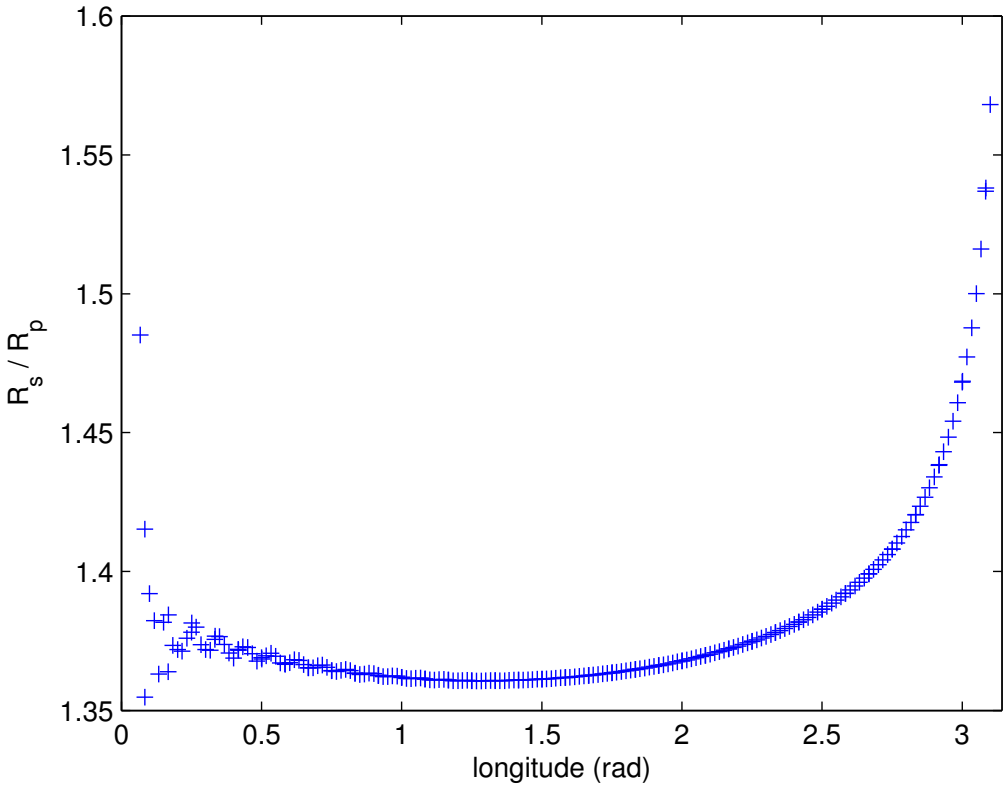

Figure 4. Sonic radius divided by planetary radius for a Neptune-like planet, as a function of the longitude, at the equator. Note that the transonic surface is not symmetric about the sub-stellar point (located at a longitude of $\pi/2$).

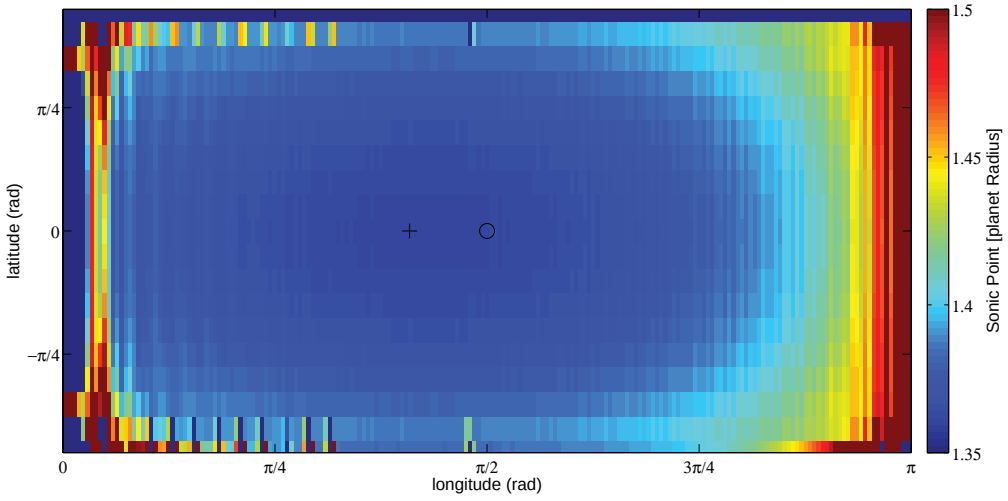

Figure 5. 2D map of sonic radius divided by planetary radius for a Netpune-like planet, as a function of longitudes (day-side only, 0 is dawn) and latitudes (from south pole to north pole, 0 is at equator). The circle indicates the substellar point, and the cross indicates the minimum sonic radius at the equator. The minimum sonic radius is offset from the substellar point by an angle of approximatively 12°.

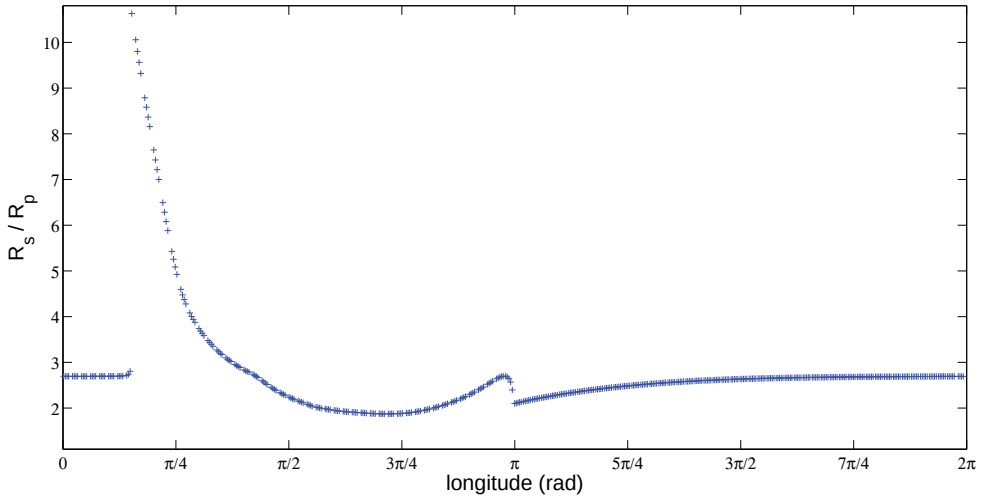

Figure 6. sonic radius divided by planetary radius for a pre-evaporation Kepler 36 planet.

helium. Because of the close proximity of the pair of planets and the star, the atmospheres of the formers undergo hydrodynamical escape, mainly during the first 10^8 yr, when the stellar flux is stronger. The core of the inner planet being less massive, it is unable to keep its atmosphere, and only the dense rocky core remains, which we observe today. The outer planet manages to retain an extended gaseous envelope, resulting in an observed low mean density. The two planets of the Kepler 36 system are also very close to a 7:6 mean motion resonance. In this paper we study the possibility for the inner planet to have been slightly shifted out of the resonance under the action of the torque exerted by its own evaporating atmosphere.

We conduct hydrodynamical simulations similar to the ones presented above, for a planet consisting of a rocky core of 4.45 $M_\oplus$ and an atmosphere whose mass is 22% of the core mass, and extends to 10 $R_\oplus$, in agreement to the model by Lopez & Fortney (2013). It receives a flux of 2.2×10^4 erg s^{-1} cm^{-2} at 0.12 AU. The sonic radius as a function of longitudes, at the equator, is presented in figure 6, and includes both day and night sides. The minimum sonic point is largely offset from the substellar point, in the East direction. On the night side, the atmosphere does not entirely cool down and a wind still exists because of the temperature at the base of the atmosphere, which is set to 1000 K in our simulations. At a radius $R = 3R_p$ which encompasses most of the sonic surface, we find the mass loss to be 5.6 10^{12} g s^{-1}. In this case we find the offset angle to be relatively small, $\theta_{lag} = 5°$. From equation (10) we estimate that the resulting drift in semi-major axis would be of 0.5%.

5.2 N-body simulations

Using a simple 3 body code (described in more detail by Quillen et al. 2013) that checks for collisions between bodies and allows forced migration via parameters $\dot{a}$ and $\dot{e}$, we can explore Kepler 36 scenarios that include mass loss accompanied by a torque. We integrate a few body system under the influence of gravity (two planets and the central star) and include a Stokes drag-like form for dissipation that induces both migration and eccentricity damping. The drag gives a force per unit mass in the form adopted by Beaugé et al. (2006). This form has previously been used to model disk-mediated migration (Lee & Peale 2002). Here we use the same form (and code) to model migration due to a wind-evaporation induced torque. We use a 4th order adaptive step-size Hermite integrator (that described by Makino & Aarseth 1992) with the addition of the drag forces and mass loss.

Kepler 36b has a density $\rho_b = 7.46$ g cm^{-3} whereas Kepler 36c has $\rho_c = 0.89$g cm^{-3}. Kepler 36b is the lighter denser planet, suggesting that it could have lost much of its mass in a wind (Lopez & Fortney 2013; Owen & Wu 2013). If the torque on the planet was positive during evaporative wind loss then the planet would have migrated outward, pushing it closer to Kepler 36c. This would have pushed the system deeper into the 7:6 resonance rather than pulling it slightly out of resonance (Deck et al. 2012). The period ratio is $P_c/P_b = 1.1733$ and $\Delta = P_c/P_b 6/7 - 1 = 0.0057$ using periods listed by Carter et al. (2012).

The system is just slightly outside of resonance with the separation between the two bodies larger than that of exact resonance (Carter et al. 2012; Deck et al. 2012). The two planets in this system could not have migrated much further apart as that would have made the system unstable.

Either, a wind from Kepler 36b did not exert much in the way of torque, or the wind moved the planet only slightly inward rather than outward.

We show a migration scenario for Kepler 36 in Figure 7. Mass loss is predicted to take place more rapidly and first from Kepler 36b. Once Kepler 36b has lost most of its envelope Kepler 36 c can slowly continue to loose mass.

Dissipation in planets from variations in the tidal force from the central star can slowly cause orbits of planet pairs in mean motion resonance to diverge (Papaloizou 2011; Delisle et al. 2012; Lithwick & Wu 2012; Batygin & Morbidelli 2013; Lee et al. 2013). Tidal dissipation is a mechanism that could account for the many near resonant Kepler planet pairs (Lithwick & Wu 2012; Batygin & Morbidelli 2013; Lee et al. 2013). Quillen et al. (2013) found (following

Lee et al. 2013) that it was difficult to account for the distance of the Kepler 36 system from the 7:6 resonance (assuming it was originally left there) using tidal forces alone (though the effect of larger planet radii and masses at earlier times and prior to evaporation was not taken into account).

Some models of tidal evolution predict low eccentricity after escape from resonance (Lithwick & Wu 2012) (with the exception of the scenario by Delisle et al. 2012). However the Kepler 36 system is near some second order resonances and, if there was divergent evolution, a resonance crossing could perhaps have lifted the eccentricity of the two planets to near their current values ~ 0.02 (Carter et al. 2012).

Kepler 36 is a radius right around where it is X-ray dominated and so the wind itself could have lifted the eccentricity slightly, perhaps, though maybe this presents a problem for pulling it out of resonance.

While second order resonance crossing (due to drift caused by an evaporative wind) presents a possible explanation for Kepler 36's eccentricity, lower index resonances such as the 3:2 are more distant from second order resonances. Only if the wind increases the eccentricity could non-zero eccentricities in lower index resonances be related to orbital variations associated with an evaporative wind.

6 SPIN EVOLUTION

In this section we give an estimate of the how the evaporative wind could affect the spin evolution of the planet. The torque on the planet itself we estimate as

$$\tau_s \sim \dot{M}(v_{zonal} - R_p\Omega_p)R_p \tag{22}$$

where v_{zonal} is the atmosphere circulation velocity and we assume that the wind is launched at a radius that is not significantly different than R_p. Here Ω_p is the spin of the planet. Assuming that $v_{zonal} > R_p\Omega_p$ and after time Δt a change in planet spin of

$$\Delta\Omega_p \sim \frac{\dot{M}\Delta t}{M_p}\frac{v_{zonal}}{R_p}\frac{1}{\alpha_p} \tag{23}$$

where the planet's moment of inertia is $I_p = \alpha_p M_p R_p^2$.

7 SUMMARY AND DISCUSSION

Evaporative winds driven from close-in planet by EUV and X-ray radiation from a star are unlikely to be isotropic. If the upper atmosphere of a wind undergoing heavy mass loss is

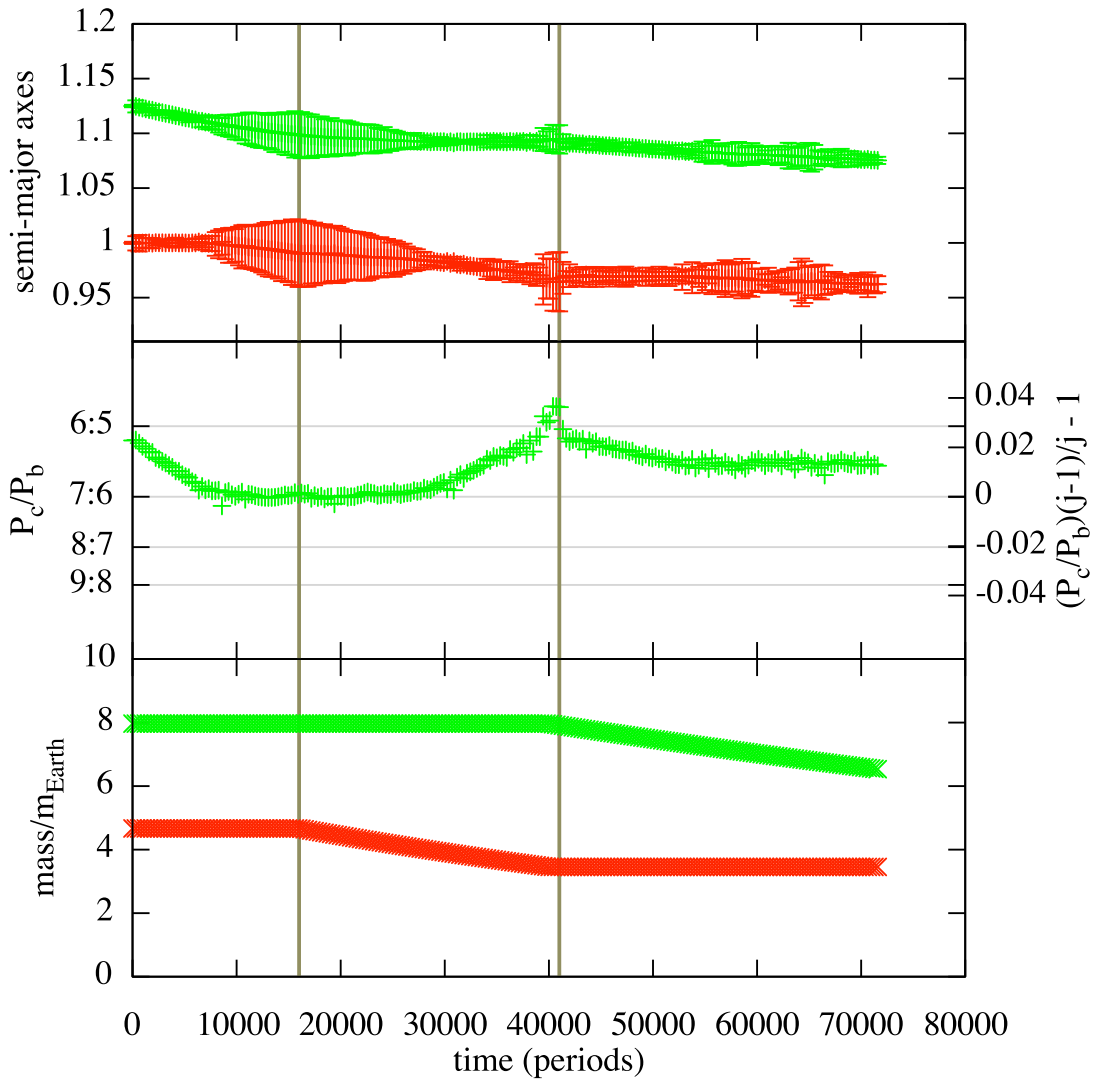

Figure 7. Mass loss from Kepler 36.

circulating with respect to a tidally locked planet, then we estimate that there would be a lag on the dawn side between the time the upper atmosphere is illuminated by starlight and when a newly launched wind becomes transonic. This results in a momentum flux on the planet. A planet that loses a significant fraction of its mass could drift by a small amount in semi-major axis (at most 10% of its semi-major axis). By estimating wind launch timescales we find that only in a narrow regime of planet radius, mass and UV + X-ray flux can the lag angle be significant or important. Consequently only in rare cases could a planet's orbit (or eccentricity) be effected by the wind's torque.

Our 1D, time-dependent, hydrodynamical simulations have shown that for a close-in, Neptune-like planet, the anisotropic torque exerted by the wind does not strongly affect the

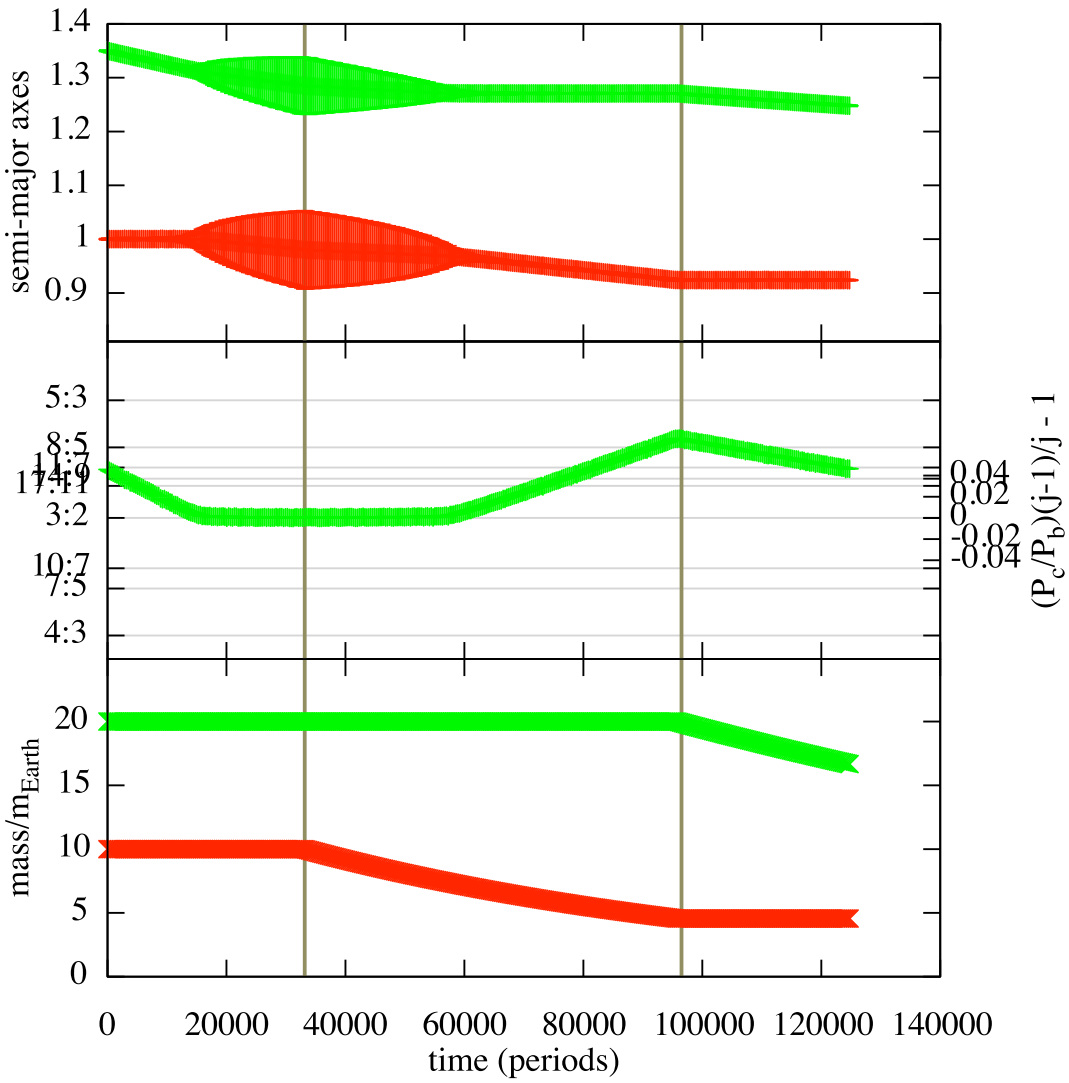

Figure 8. Mass loss from a pair of planets in 3:2.

semi-major axis of the planet. The effect is slightly more significant in the case of Kepler 36b. The small distance in semi-major axis that the wind could cause might be significant in near-resonant systems. Small amounts of drifting coupled with mass loss could possibly account for Kepler 36 b,c's distance from the 7:6 resonance and current eccentricity.

This work was initiated during the International Summer-Institute for Modeling in Astrophysics (ISIMA) in 2014, hosted at CITA at the University of Toronto. This work was in part supported by NASA grant NNX13AI27G. We also thank Kristen Menou, Linda Strubbe, Pascale Garaud, Jeremy Leconte, Yanqin Wu, Subu Mohanty and Man-Hoi Lee for helpful discussions and correspondence.

REFERENCES

Batalha, N. M., Borucki, W. J., Bryson, S. T., et al. 2011, ApJ, 729, 27

Batalha, N. M. et al. 2013, ApJS, 204, 24

Batygin, K., & Morbidelli, A. 2013, AJ, 145, 1 Dissipative Divergence of Resonant Orbits

Beauge, C., Michtchenko , T. A., & Ferraz-Mello, S. 2006, MNRAS, 365, 1160

Bodenheimer, P., Lin, D. N. C., & Mardling, R. A. 2001, ApJ, 548, 466 On the tidal inflation of short-period extrasolar planets

Bottke, W.F., Vokrouhlický, D., Rubincam, D.P. and Nesvorný, D. 2006, The Yarkovsky and YORP effects: Implications for asteroid dynamics, Ann. Rev. Earth Planet. Sci. 34, 157191.

Boué, G., Figueira, P., Correia, A. C. M., & Santos, N. C. 2012, A&A, 537, L3 Orbital migration induced by anisotropic evaporation. Can hot Jupiters form hot Neptunes?

Burns, J. A. 1976, American Journal of Physics 44, 944 (1976); doi: 10.1119/1.10237 Elementary derivation of the perturbation equations of celestial mechanics

Carter, J. A., Agol, E., Chaplin, W. J., Basu, S., Bedding, T. R., Buchhave, L. A., et al. 2012, Science, 337, 556 Kepler-36: A Pair of Planets with Neighboring Orbits and Dissimilar Densities

Ciardi, D. R., Fabrycky, D. C., Ford, E. B., Gautier III, T. N., Howell, S. B., Lissauer, J. J., Ragozzine, D., Rowe, J. F. 2013, ApJ, 763, 41 On the Relative size of planets within Kepler Multiple-Candidate systems

Cranmer, S. R. 2004, American Journal of Physics, Volume 72, Issue 11, pp. 1397-1403. New views of the solar wind with the Lambert W function

Cowan, N. B., Agol, E. 2011, ApJ, 726, 82 A Model for Thermal Phase Variations of Circular and Eccentric Exoplanets

Cowan, N. B., & Agol, E. 2011, ApJ, 729, 54 The Statistics of Albedo and Heat Recirculation on Hot Exoplanets

Cunha, D., Correia, A. C. M., & Laskar, J. 2014, arXiv1406.4544 Spin evolution of Earth-sized exoplanets, including atmospheric tides and core-mantle friction

Deck, K. M., Holman, M. J., Agol, E., Carter, J. A., Lissauer, J. J., Ragozzine, D., & Winn, J. N. 2012, ApJ, 755, L21 Rapid Dynamical Chaos in an Exoplanetary System

Delisle, J.-B., Laskar, J., Correia, A. C. M., Boué, G. 2012, A&A, 546, 71 Dissipation in planar resonant planetary systems

Delisle, J.-B., Laskar, J., & Correia, A. C. M. 2014, A&A, 566, 137 Resonance breaking due to dissipation in planar planetary systems

Delisle, J.-B., & Laskar, J. 2014, A&A, in press http://arxiv.org/abs/1406.0694 Tidal dissipation and the formation of Kepler near-resonant planets

Erkaev N. V., Kulikov, Y. N., Lammer, H., Selsis, F., Langmayr, D., Jaritz, G. F., & Biernat, H. K. 2007, A&A, 472, 329 Roche lobe effects on the atmospheric loss from "Hot Jupiters"

Fabrycky, D. et al. 2014, accepted for publication in ApJS, arXiv1202.6328 Architecture of Kepler's Multi-transiting Systems: II. New investigations with twice as many candidates

Ford, E. B. & Rasio, F. A. 2008, ApJ, 686, 621 Origins of Eccentric Extrasolar Planets: Testing the Planet-Planet Scattering Model

Guti/'errez, P.J., Ortiz, J. L., Rodrigo, R., Lopez-Moreno, J.J., Jorda, L., 2002. Evolution of the rotational state of irregular cometary nuclei. Earth Moon Planets 90, 239-247.

Hadden, S. & Lithwick, Y. 2014, ApJ, 787, 80 Densities and Eccentricities of 139 Kepler Planets from Transit Time Variations

Heng, K., Menou, K., Phillips, P. J. 2011 MNRAS, 413, 2380-2402 Atmospheric circulation of tidally locked exoplanets: a suite of benchmark tests for dynamical solvers

Howe, A. R., Burrows, A., & Verne, W. 2014, ApJ, 787, 173 Mass-radius Relations and Core-envelope Decompositions of Super-Earths and Sub-Neptunes

Hut, P. 1981,A&A, 99, 126 Tidal evolution in close binary systems

Iorio L., 2012, New Astron., 17, 356

Jontof-Hutter, D., Lissauer, J. J., Rowe, J. F., & Fabrycky, D. C. 2014, ApJ, 785, 15 Kepler-79's Low Density Planets

Koskinen, T. T., Cho, J. Y.-J., Achilleos, N. Aylward, A. D. 2010, ApJ, 722, 178

Lecavelier des Etangs, A., Ehrenreich, D., Vidal-Madjar, A., Ballester, G. E., Désert, J.-M., Ferlet, R., Hébrard, G., Sing, D. K., Tchakoumegni, K.-O., & Udry, S. 2010, A&A, 514, 72

Lee, M. H., & Peale, S. J. 2002, ApJ, 567, 596Dynamics and Origin of the 2:1 Orbital Resonances of the GJ 876 Planets

Lee, M. H., Fabrycky, D., & Lin, D. N. C. 2013, ApJ, 774, 52 Are the Kepler Near-resonance Planet Pairs due to Tidal Dissipation?

Lithwick, Y., & Wu, Y. 2012, ApJ, 756, L11 Resonant Repulsion of Kepler Planet Pairs

Lopez, E., & Fortney, J. 2013, ApJ, 776, 2 The Role of Core Mass in Controlling Evapora-

tion: the Kepler Radius Distribution and the Kepler-36 Density Dichotomy

Lubow, S. H., Tout, C. A., & Livio, M. 1997, ApJ, 484, 866 Resonant Tides in Close Orbiting Planets

Makino, J., & Aarseth, S. J. 1992, PASJ, 44, 141

Matsumura, S., Tadeka, G. & Rasio, F. A. 2008, ApJL, 686, L29 On the Origins of Eccentric Close-In Planets

Matsumura, S., Peale, S. J. & Rasio, F. A. 2013, ApJ, 725, 1995Tidal Evolution of Close-in Planets

Menou, K. 2012, ApJ, 744, L16 Atmospheric Circulation and Composition of GJ1214b

Neishtadt, A. I., Scheeres, D. J., Sidorenko, V. V., Stooke, P. J., Vasiliev, A. A. 2003, The Influence of Reactive Torques on Comet Nucleus Rotation, Celestial Mechanics and Dynamical Astronomy, 86, 249-275.

Nesvorný, D., Kipping, D. M., Buchhave, L. A., Bakos, . A., Hartman, J., & Schmitt, A. R. 2012, Science, 336, 1133 The Detection and Characterization of a Nontransiting Planet by Transit Timing Variations

Owen, J. E. & Adams, F. 2014, arxiv:1408.3636, accepted for publication in MNRAS Magnetically controlled mass loss from extra solar planets in close orbits

Owen, J. E. & Wu, Y. 2013, ApJ, 775, 105 Kepler planets: a tale of evaporation

Owen, J. E. & Jackson, A. P. 2012, MNRAS, 425, 2931 Planetary evaporation by UV & X-ray radiation: basic hydrodynamics

Parker, E. N. 1958, ApJ, 128, 664

Papaloizou, J. C. B. 2011, Celest. Mech. Dyn. Astron., 111, 83

Parker, E. N. 1965, Space Sci. Rev., 4, 666

Quillen, A. C. Bodman, E. Moore, A. 2013, MNRAS, 435, 2256 Origin Scenarios for the Kepler 36 Planetary System

Rauscher, E., & Kempton, E. M. R. 2014, arXiv1402.4833 The Atmospheric Circulation and Observable Properties of Non-Synchronously Rotating Hot Jupiters

Rodriguez, A., Callegari, N., Michtchenko, T. A., & Hussmann, H. 2012, MNRAS, 427, 2239 Spin-orbit coupling for tidally evolving super-Earths

Showman, A. P. & Polvani, L. M. 2011, ApJ, 738, 71 Equatorial Superrotation on Tidally Locked Exoplanets

Shu, F. H. 1992, Gas Dynamics (Mill Valley: Univ. Science Books)

Spitzer, L. 1978, Physics Processes in the Interstellar Medium (New York: Wiley)

Stone, J. M. & Norman, M. L., 1992, ApJS, 80, 753

Veras, D., Hadjidemetriou, J. D., & Tout, C. A. 2013, MNRAS, 435, 2416 An exoplanet's response to anisotropic stellar mass loss during birth and death

Vidal-Madjar, A., Lecavelier des Etangs, A., Désert, J.-M., Ballester, G. E., Ferlet, R., Hébrard, G., & Mayor, M., 2003, Nature, 422,143

Wu, Y., & Lithwick, Y. 2013, ApJ, 772, 74 Density and Eccentricity of Kepler Planets

APPENDIX A: ECCENTRICITY AND INCLINATION EVOLUTION

In this section we compute the rate of change of eccentricity and inclination caused by a wind's momentum loss rate. Following Burns et al. (1976), we average the force per unit mass exerted by the wind on the planet over the planet's orbit.

A wind that carries momentum at a rate $\dot{\mathbf{P}}$ exerts a force per unit mass $\mathbf{F}_w = \dot{\mathbf{P}}/M_p$ on the planet. Following Burns et al. (1976) we decompose the force per unit mass from the wind into components

$$\mathbf{F}_w = T\hat{\boldsymbol{\theta}} + R\hat{\mathbf{r}} + N\hat{\mathbf{z}} \tag{A1}$$

in spherical coordinates defined by the planet's position $r\hat{\mathbf{r}}$ and with $\hat{\mathbf{z}}$ aligned with the orbital angular momentum vector. Here T, R, N have units of acceleration. The work per unit mass (change in orbital energy per unit mass) is

$$\dot{E}_o = \mathbf{v} \cdot \mathbf{F}_w = \dot{r}R + r\dot{\theta}T. \tag{A2}$$

The change in orbital energy directly gives an estimate for the drift rate in semi-major axis

$$\dot{a}_p = \frac{2a_p^2}{GM_*}(\dot{r}R + r\dot{\theta}T). \tag{A3}$$

At low eccentricity, the timescale for drift in semi-major axisis

$$\tau_a \equiv \frac{a}{\dot{a}_p} \approx n^{-1}\frac{GM_*}{2Ta^2} \tag{A4}$$

where n is the planet's mean motion. Because $\dot{a}_p$ is non-zero at zero eccentricity, we ignore the sensitivity of the migration rate to eccentricity.

A1 Eccentricity evolution

For the eccentricity evolution

$$\begin{aligned} n^{-1}\frac{d}{dt}\frac{e^2}{2} &= \frac{2HE_o}{n}\dot{H} + \frac{H^2}{n}\dot{E}_o \\ &= \frac{2HE_o rT}{n} + \frac{H^2}{n}(\dot{r}R + r\dot{\theta}T) \end{aligned} \tag{A5}$$

where the angular momentum per unit mass reads

$$\mathbf{H} = na_p^2 y\hat{\mathbf{z}}. \tag{A6}$$

Here e is the planet's eccentricity and $y \equiv \sqrt{1-e^2}$. Whereas $\dot{a}_p$ contains a non-zero eccentricity independent term, eccentricity damping or growth only takes place if there is eccentricity and both terms in equation A5 are needed to calculate this rate. The torque $\dot{\mathbf{H}} = \mathbf{r} \times \mathbf{F}$, and the magnitude $\dot{H} = rT$ in terms of the tangential force component. The radius from the star is

$$r = a_p(1 - e\cos E) \tag{A7}$$

with E the eccentric anomaly. The mean anomaly M and the eccentric anomaly are related by Kepler's equation

$$M = E - e\sin E. \tag{A8}$$

The mean motion

$$n = \dot{E}(1 - e\cos E). \tag{A9}$$

Inserting these two equations into our expression for radius, we get

$$\dot{r} = a_p e\sin E\dot{E} = \frac{a_p e\sin E n}{1 - e\cos E}. \tag{A10}$$

Using $H = r^2\dot{\theta}$ we find

$$r\dot{\theta} = \frac{na_p^2 y}{r} = \frac{na_p y}{1 - e\cos E} \tag{A11}$$

Putting expressions that depend on the eccentric anomaly into equation (A5), we find for the eccentricity evolution

$$n^{-1}\frac{d}{dt}\frac{e^2}{2} = \frac{a_p^2}{GM_*}\left[-T(1 - e\cos E)y + \frac{Ty^3}{1 - e\cos E} + \frac{Re\sin Ey^2}{1 - e\cos E}\right] \tag{A12}$$

This is equivalent to equation (28) by Burns et al. (1976) but this is written in terms of the eccentric anomaly so it can more easily be integrated.

Let us assume that R and T both depend on radius in the same way so that

$$T \equiv R\sin\theta_w \tag{A13}$$

with θ_w the angle of the integrated outflow momentum. This means that $T < R$.

$$n^{-1}\frac{d}{dt}\frac{e^2}{2} = \frac{Ra_p^2}{GM_*}\left[\sin\theta_w y\left(-(1-e\cos E)+\frac{y^2}{1-e\cos E}\right)\right.$$
$$\left.+\frac{e\sin E y^2}{1-e\cos E}\right] \quad \text{(A14)}$$

Differentiating Kepler's equation

$$dM = ndt = dE(1-e\cos E) \quad \text{(A15)}$$

and we average equation (A14) over a rotation period

$$\langle n^{-1}\frac{d}{dt}\frac{e^2}{2}\rangle = \frac{1}{2\pi}\frac{a_p^2}{GM_*}\int_0^{2\pi} dE\ R(E)$$
$$\left[\sin\theta_w y(2e\cos E - e^2\cos^2 E - e^2)\right.$$
$$\left.+e\sin E y^2\right] \quad \text{(A16)}$$

There is no eccentricity damping unless there is some eccentricity. Hereafter we drop the brackets and discuss the orbit averaged eccentricity evolution.

Assume that with a low order eccentricity expansion we can write

$$R(E) \sim \bar{R}(1 + r_c\cos E + r_s\sin E) \quad \text{(A17)}$$

where r_c and r_s are unit-less but could depend on eccentricity. If the momentum flux $R(E) \propto r^{-\beta}$ then to first order $R(E) \propto (1-\beta e\cos E)$ and $r_s = 0$. If there is a seasonal lag, then we might get nonzero r_s term. Integrating equation (A16) we find

$$n^{-1}\frac{d}{dt}\frac{e^2}{2} \sim \frac{\bar{R}a_p^2}{GM_*}e\left(\sin\theta_w\left(-\frac{3}{2}e + r_c\right) + \frac{r_s}{2}\right) \quad \text{(A18)}$$

and we have dropped terms higher than second order in eccentricity because equation (A17) is a low order approximation.

If the wind momentum flux depends inversely on radius then $r_c \sim e$ and

$$n^{-1}\frac{d}{dt}\frac{e^2}{2} \sim -\frac{\bar{R}a_p^2}{GM_*}\frac{e^2}{2}\sin\theta_w \quad \text{(A19)}$$

and we expect eccentricity damping. If the wind momentum flux depends inversely on the square of radius then $r_c \sim 2e$ and

$$n^{-1}\frac{d}{dt}\frac{e^2}{2} \sim \frac{\bar{R}a_p^2}{GM_*}\frac{e^2}{2}\sin\theta_w \quad \text{(A20)}$$

and we expect an increase in eccentricity. Owen & Jackson (2012) predict that X-ray driven winds have mass loss rate proportional to r^{-2} and EUV driven winds have mass loss rates proportional to r^{-1}. This suggests that for planets within 0.1 AU of a star, the wind could cause the orbital eccentricity to increase whereas external to this the eccentricity would be damped.

And in both cases the timescale for eccentricity variation is similar to

$$\tau_e = \frac{e^2}{de^2/dt} \sim \frac{1}{n \sin\theta_w} \frac{GM_*}{\bar{R}a^2} \tag{A21}$$

Our expression for the eccentricity damping (or increase) timescale and eccentricity evolution rate depend on $\bar{R}a_p^2/(GM_*) = \bar{R}$ and $\bar{R}$ is in units of acceleration as it is is force per unit mass. This implies that

$$\bar{R} \sim \frac{\dot{M} v_w}{M_p} \tag{A22}$$

or

$$\frac{\bar{R}a_p^2}{GM_*} = \frac{v_w}{v_c} \frac{\dot{M}}{M_p n} \tag{A23}$$

which depends on the ratio of the wind outflow velocity and orbital speed and the mass loss rate related to the fraction of mass lost per orbital period. The torque we previously estimated $\tau_w = M_p T$ giving

$$\sin\theta_w = \frac{\tau_w}{\dot{M} v_w} \tag{A24}$$

Putting these together , we find:

$$\tau_e = \frac{e^2}{de^2/dt} = \frac{1}{\sin\theta_w} \frac{v_c}{v_w} \frac{M_p}{\dot{M}} \tag{A25}$$

and $\tau_e \sim \tau_a$. We find that the ratio commonly used to describe migration rates, $K \equiv \tau_a/\tau_e$ (Lee & Peale 2002), is of order unity for evaporative winds.

A2 Inclination evolution

The rate of inclination change depends only on the vertical force component N, (Burns et al. 1976, their equation 32)

$$\frac{di}{dt} = \frac{rN}{na^2 y} \cos(\omega + f) \tag{A26}$$

where ω is the argument of pericenter and f is the true anomaly. Using relations between mean anomaly and true anomaly

$$r\cos f = a(\cos E - e) \tag{A27}$$

$$r\sin f = ay \sin E \tag{A28}$$

we find

$$n^{-1}\frac{di}{dt} = \frac{Na^2}{GM_*} \left[y^{-1} \cos\omega(\cos E - e) - \sin\omega \sin E \right] \tag{A29}$$

Using Kepler's equation and averaging over the orbit

$$n^{-1}\langle\frac{di}{dt}\rangle = \frac{1}{2\pi}\int dE \frac{N(E,\omega)a^2}{GM_*}(1-e\cos E)\times \left[y^{-1}\cos\omega(\cos E - e) - \sin\omega\sin E\right] \quad \text{(A30)}$$

Hereafter we discuss the orbit averaged rate of change in the inclination.

A planet at zero eccentricity in a 2:1 spin-orbit resonance but with a misaligned magnetic pole with tilt angle ω_p, has a non-zero vertical component of force per unit mass N. Roughly

$$N \sim \dot{M} c_{EUV} \sin 2\omega_p \cos f. \quad \text{(A31)}$$

We use $\sin 2\omega_p$ to take into account the illumination of the pole required to launch a wind along the polar axis. Ignoring the argument of pericenter as we assume a low eccentricity, by integrating equation A26 over the orbit we find

$$\frac{di}{dt} \sim n\frac{\dot{M} c_{EUV}\sin 2\omega_p}{2M_p}\frac{a^2}{GM_*}. \quad \text{(A32)}$$

And a total inclination change over the time for wind evaporation

$$\Delta i \sim \frac{c_{EUV}}{v_c}\frac{\Delta M_p}{M_p}\sin 2\omega_p \quad \text{(A33)}$$

but only if the magnetic pole remains misaligned with the spin axis. The total change in inclination is similar to that the fraction in semi-major axis (equation 10) except there is a factor of $\sin 2\omega_p$ dependent on the obliquity of the magnetic pole.

For a tidally locked but eccentric planet with a misaligned magnetic axis we can assume that N depends on radius alone. To low order in eccentricity let us more generally assume that

$$N = \bar{N}(1 + n_c\cos E + n_s \sin E) \quad \text{(A34)}$$

where n_c and n_s could depend on eccentricity. Integrating equation A30 we find

$$n^{-1}\frac{di}{dt} = \frac{\bar{N}a^2}{GM_*}\times \left[y^{-1}\cos\omega\left(-\frac{3}{2}e + \frac{n_c}{2}(1+e^2)\right) - \sin\omega\frac{n_s}{2}\right] \quad \text{(A35)}$$

If $N \propto r^{-1}$ then $n_c = e$ and $n_s = 0$. In this case

$$n^{-1}\frac{di}{dt} \sim -e\frac{\bar{N}a^2}{GM_*}\cos\omega \quad \text{(A36)}$$

If $N \propto r^{-2}$ then $n_c = 2e$, $n_s = 0$ and

$$n^{-1}\frac{di}{dt} \sim -\frac{e}{2}\frac{\bar{N}a^2}{GM_*}\cos\omega \quad \text{(A37)}$$

For this setting we can again estimate the total inclination change with $\bar{N} \sim \dot{M} c_{EUV}\sin 2\omega_p$

and

$$\Delta i \sim \frac{c_{EUV}}{v_c}\frac{\Delta M_p}{M_p} e \sin 2\omega_p. \tag{A38}$$

similar to equation A33 but with a factor of eccentricity.

APPENDIX B: FORCE OF A WIND ON A PLANET

Consider a planet of mass M_p moving at velocity v_p in a frame co-rotating with the Keplerian orbit of the planet, which is surrounded by a evaporative wind which is a fluid system with density field ρ and velocity field $\mathbf{u}$. The conservation of momentum states:

$$\frac{\mathrm{d}}{\mathrm{d}t}\left(M_p v_p\right) + \int_V \mathrm{d}V \left[\frac{\partial}{\partial t}\left(\rho\mathbf{u}\right) + \nabla\cdot\left(\rho\mathbf{u}\mathbf{u}\right) + \nabla P + \rho\nabla\psi_g\right] = F_{\mathrm{rot}} \tag{B1}$$

where F_{rot} is the force terms from a non-inertial frame, which should be small on both the planet and wind, such that $F_{rot} \approx 0$. The eulerian derivative of $\rho\mathbf{u}$ is zero for a steady-state wind, so using the divergence theorem one finds:

$$\frac{\mathrm{d}}{\mathrm{d}t}\left(M_p V_p\right)_i = -\int_{\partial V} \rho u_i u_j \mathrm{d}A^j - \int_{\partial V} P \mathrm{d}A_i - \int_V \mathrm{d}V \rho\partial_i\psi_g. \tag{B2}$$